THE JOURNAL OF PHYSICAL CHEMISTRY B

Article

pubs.acs.org/JPCB

Thioflavin T and Its Photoirradiative Derivatives: Exploring Their Spectroscopic Properties in the Absence and Presence of Amyloid Fibrils

Jack C.-C. Hsu,[†,∥] Eric H.-L. Chen,[†,∥] Robert C. Snoeberger, III,[‡] Frederick Y. Luh,[†] T.-S. Lim,[§] C.-P. Hsu,[‡] and Rita P.-Y. Chen*[,†]

[†]Institute of Biological Chemistry, Academia Sinica, Taipei, 11529, Taiwan

[‡]Institute of Chemistry, Academia Sinica, Taipei, 11529, Taiwan

[§]Department of Physics, Tunghai University, Taichung 407, Taiwan

Supporting Information

ABSTRACT: In this work, we found that, during storage or after UV irradiation, ThT is demethylated or oxidized, forming three derivatives. These three derivatives were purified by high performance liquid chromatography and characterized by mass and nuclear magnetic resonance spectroscopy and the spectroscopic properties of pure ThT and the derivatives carefully compared. Our results show that the emission peak at 450 nm results from oxidized ThT and not from the monomeric form of ThT, as previously proposed. The partial conversion of ThT into oxidized and demethylated derivatives has an effect on amyloid detection using ThT assay. Irradiated ThT has the same lag time as pure ThT in the amyloidogenesis of insulin, but the intensity of the emitted fluorescence is significantly decreased.

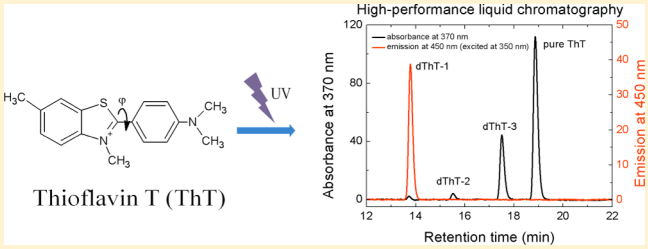

INTRODUCTION

Protein misfolding not only correlates with biofunctional loss but also induces many diseases, such as Alzheimer's disease, transmissible spongiform encephalopathy, Parkinson's disease, and systemic amyloidosis, due to the accumulation of toxic β-sheet rich protein aggregates known as amyloids.[1−5] The term "amyloid" comes from its special dye-binding properties, similar to amylose binding with iodine.[6−8] Since amyloid is a major pathologic characteristic of these diseases, its identification is very important. For histological staining, Congo red or thioflavin S is commonly used to identify amyloid accumulation in tissues.[9,10] In vitro, circular dichroism spectroscopy, Fourier transform infrared spectroscopy, and fluorescence spectroscopy after binding to thioflavin T (ThT) have been used to quantify the amount of amyloid based on its cross-β structural character, while electron microscopy, atomic force microscopy, and X-ray fibril diffraction are used to examine its filamentous morphology.[11−21] Of these techniques, the ThT binding assay is the most popular and sensitive technique for detecting and monitoring the progression of amyloid fibril formation.[22,23] Pure ThT has a strong absorption peak centered at 412 nm and a low fluorescence emission at 487 nm when excited at 412 nm. On binding to amyloid fibrils, the absorption maximum is red-shifted to 442 nm and the ThT/amyloid complex emits strong fluorescence at 478 nm when excited at 442 nm. Using the dye ATTO-425 as a standard, the fluorescence quantum yield (Q.Y.) of ThT has been measured in water (Q.Y. < 10^{-3}),[24] rigid isotropic solution (Q.Y. ∼ 0.28), and in the presence of amyloid fibrils (Q.Y. ∼ 0.43).[25] This fluorescence enhancement on formation of the ThT/amyloid complex makes ThT a useful extrinsic fluorescent sensor for amyloid. However, it was reported recently that ThT can also bind to non-amyloid amorphous β-aggregates[11] and to a native helical protein, such as human serum albumin.[26]

The structural, chemical, and photophysical properties of ThT have recently been extensively studied, and several models have been proposed to explain the origin of the fluorescence enhancement seen on binding to amyloid. The "excimer model" suggested that the presence of a short-wavelength emission band at 450 nm was attributed to the fluorescence of the monomeric form of ThT and the strong red-shifted excimer emission at 478 nm is due to amyloid binding to the ThT dimer.[27−32] This model was supported by the formation of columnar stacks in the crystal structure of ThT[33] and the finding that synthesized ThT dimers bind much more readily to amyloid fibrils than ThT monomers.[27,34] Except dimer, a micelle formation was also proposed. Using electric conductivity and atomic force microscopy methods, Khurana et al. proposed the formation of ThT micelles in the interior of amyloid fibrils.[35]

Some investigators have used special materials, including β-cyclodextrin, porous silicon, and reverse micelles, to confine

Received: September 20, 2012
Revised: March 1, 2013
Published: March 4, 2013

   dx.doi.org/10.1021/jp309331u | J. Phys. Chem. B 2013, 117, 3459−3468

ThT in a nanocavity and studied ThT fluorescence enhancement in these materials.[30,36−39] The results show that the fluorescence intensity of ThT is increased in a nanocavity, implying that binding of ThT to the specific amino acid sequence of an amyloid fiber is not essential. The "molecular rotor" model was proposed to explain the fluorescence enhancement effect of ThT on binding to amyloid.[40] This model suggests that the increased fluorescence quantum yield is due to the rotational restriction of the benzothiazole and dimethylaminobenzene rings of ThT, trapping the excited state in the emissive locally excited state (LE).[41,42] The bond connecting the benzothiazole and dimethylaminobenzene rings of ThT can rotate, and one rotamer with a torsion angle of 90° is considered as the twisted internal charge transfer (TICT) state, whereas the LE state is more planar than the TICT state.[40,43,44] Rotation to the twisted state is more favorable in a polar solvent, in which the twisted state induces a charge separation between these two rings.[45] The photophysics of ThT with/without amyloid fibrils strongly correlates with the photoinduced TICT state. The molecular rotor model was supported by the findings *vide infra*: Kitts et al. provided data suggesting that ThT is incorporated into amyloid fibrils in the monomeric form;[46] ThT behaves like a molecular rotor, and its rotation is controlled by its microenvironment;[36] increasing solvent viscosity or rigidity of the ThT microenvironment (β-sheet groove) results in fluorescence enhancement.[47,48]

In this paper, we report that ThT forms three kinds of derivatives during storage and on photoirradiation. Pure ThT and the three derivatives were isolated by reverse-phase high-performance liquid chromatography (HPLC) and their structures and spectroscopic properties examined and compared. One derivative, named dThT-1, was produced by ThT oxidation, while the other two derivatives were due to demethylation of ThT; that having lost two methyl substituents on the aminobenzene ring is referred to as dThT-2 and that having lost one methyl substituent as dThT-3. The spectral and chemical properties of ThT and its derivatives, such as spectrum shift, fluorescence quantum yield, fluorescence lifetime, fluorescence enhancement effect upon amyloid binding, and amyloid-binding ability, were compared. Computational modeling was used to map the potential energy surface governing the LE-to-TICT conversion process of ThT and its demethylated derivatives dThT-2 and dThT-3. Finally, the kinetics of insulin fibril formation monitored by using pure ThT was compared with that using irradiated ThT.

EXPERIMENTAL METHODS

Purification of ThT. Thioflavin T powder purchased from Sigma-Aldrich (USA) was dissolved in distilled water (Millipore, USA) and purified by reverse-phase high-performance liquid chromatography (HPLC) using a Vydac C18 column (10 mm × 250 mm) and gradients of different acetonitrile−water mixtures containing 0.1% trifluoroacetic acid (v/v) as the mobile phase (details in figure legends). Fractions containing pure ThT and its derivatives were collected, lyophilized, and stored at 4 °C. Solutions of ThT or its derivatives were freshly prepared and filtered through a syringe filter (pore size 0.22 μm, Millex GP, Millipore) before each experiment.

Preparation of Insulin Amyloid Fibrils. Insulin fibrils were produced by incubating bovine insulin (5 mg/mL, Sigma-Aldrich, USA) in fibrillization buffer (20% acetic acid and 0.5 M NaCl, pH 1.8) at 60 °C for 3 days.[49] Then, the fibril solution was centrifuged at 16 100*g* for 30 min at room temperature to separate insoluble fibrils and any remaining insulin monomer. The monomer concentration in the supernatant was determined by UV/vis spectroscopy and the fibril concentration estimated by subtracting the remaining monomer concentration from the original insulin concentration.

Irradiation of ThT and Spectral Measurements. Pure ThT was irradiated in a "merry-go-round" photoreactor PR-2000 (Pan-Chum, Taiwan) at full power (1.4 W) at room temperature for 60 min. The radiation wavelength of the photoreactor was centered on 352 nm. The concentration of pure ThT was estimated on the basis of its UV absorption at 412 nm, using an extinction coefficient of ∼34 000 M^{-1} cm^{-1} at 412 nm (Figure S1, Supporting Information).[50,51] The ThT derivatives formed after irradiation were purified by HPLC. The absorption spectra of pure ThT and its derivatives were measured in distilled water on a DU 800 UV/vis spectrophotometer (Beckman Coulter, USA), while their fluorescence emission and excitation spectra were recorded using a FluoroLog 3 spectrofluorimeter (HORIBA Jobin Yvon, France).

Computational Methods. The derivative dThT-1 was not included in the computation study because its structure could not be clearly determined. The excited electronic structure and relaxed geometry were computed by the configuration interaction singles (CIS) method on a 6-31G** basis.[52] We avoid using time-dependent density functional theory (TDDFT) because most commonly used functionals (such as B3LYP) have a serious problem in the charge-transfer state energies and corresponding potential energy surfaces.[53] Although the CIS method is known to overestimate the excitation energy of excited states[54] and has recently been shown to display a systematically larger overestimation of excitation energies for charge transfer states,[55] which happens to be the state of interest in this work, it is still more reliable for the determination of molecular structures and vibrational frequencies especially when compared to TDDFT.

The solvation energy is an important component of the excited-state potential energy surface, especially since the fluorescence measurements were performed in both aqueous and protein-bound environments. Solvation can have a non-negligible effect on the transition from the LE state to the TICT state. In fact, the computational modeling reported here showed that solvation was extremely important for understanding the photophysics. In order to include solvation, an implicit solvation model was employed to solvate the CIS excited state electronic structure in a dielectric environment. The state-specific version of the self-consistent reaction field method was used to self-consistently relax the solvent reaction field to the electronic structure of the first excited state.[56] All quantum chemical calculations were performed using the Gaussian 09 software package (*Gaussian 09*, revision A.1; Gaussian, Inc.: Wallingford, CT, 2009).

Kinetics of Fibril Formation. Bovine insulin (Sigma-Aldrich, USA) and pure ThT were dissolved separately in fibrillization buffer. Insulin solutions were freshly prepared, centrifuged at 858*g* for 10 min at room temperature, and filtered through a Millex HV 0.45 μm filter (Millipore, USA) before each experiment. Protein concentration was determined by the UV absorbance at 276 nm.[57] Pure ThT was freshly prepared in fibrillization buffer at a stock concentration of 20 μM. A 50 μL portion of the ThT solution with or without irradiation was mixed with 50 μL of insulin (0.25, 0.56, 1.05,

dx.doi.org/10.1021/jp309331u | J. Phys. Chem. B 2013, 117, 3459−3468

1.96, and 4.03 mg/mL) in 96-microwell polystyrene plates (Nalge Nunc), and the plates were incubated at 45 °C with 10 s of mechanical shaking before each measurement. Fibrillization kinetics were measured by recording the emitted fluorescence at 478 nm using a Gemini EM Microplate Reader (Molecular Devices, USA) with excitation at 412 nm. Four replicates were used for each sample.

LC-ESI-MS. The LC-ESI-MS system consisted of an ultraperformance liquid chromatography system (Ultimate 3000 RSLC, Dionex) and an electrospray ionization (ESI) source of quadrupole time-of-flight (TOF) mass spectrometer (maXis HUR-QToF system, Bruker Daltonics). The autosampler was set at 4 °C. Separation was performed by reversed-phase liquid chromatography on a BEH C18 column (2.1 × 100 mm^2, Walters). The column was equilibrated by pumping 1% solvent B (0.1% formic acid in acetonitrile) and 99% solvent A (0.1% formic acid in deionized water) for 4 min, held at 1% B for 0.5 min, raised to 60% B in 5 min, then to 90% B in 0.5 min, held at 90% B for 1.5 min, and then lowered to 1% B in 0.5 min. The flow rate was set at 0.4 mL/min using an injection volume of 2 μL. The LC-ESI-MS chromatograms were acquired in positive ion mode under the conditions of capillary voltage 4500 V, dry temperature 190 °C, dry gas flow 8 L/min, nebulizer gas 1.4 bar, and acquisition range m/z 100−1000.

Fluorescence Lifetime Measurement. Insulin fibrils prepared from 5 mg of insulin were suspended in 500 μL of water. ThT (8 μM), dThT-2 (16 μM), and dThT-3 (16 μM) were dissolved in water (a lower concentration was used for ThT because ThT has a higher absorption at 438 nm). A 20 μL portion of each dye solution was mixed with the same volume of the insulin fibril solution and then dropped onto a glass slide on which a Gene Frame (25 μL, 1.0 × 1.0 cm^2, Thermo Scientific, USA) is adhered, and then covered with a coverglass. A pulsed single mode fiber coupled diode laser (PicoQuant GmbH, LDH-P-C-440) operating at 438 nm was used as the excitation light source, with a pulse width of 90 ps, a repetition rate of 40 MHz, and a power of 1 μW. The single mode laser light was first collimated with a lens and then injected into a microscope. After being injected into the microscope, the excitation laser light was reflected by a dichroic filter (Chroma, 455DCXT) which has high reflectivity at a wavelength of 438 nm. Then, the excitation laser was focused by an objective (Olympus, UPlanFLN, 40×, 0.75 NA) onto the samples. The fluorescence of the samples was collected by the same objective. The photons emitted by the sample were detected by an avalanche photodiode (APD) operating in photon counting mode. A long-pass filter (Chroma, HQ455LP) was put before the APD to block reflected and scattered excitation light from samples. Fluorescence decay curves were measured using a time-correlated single-photon counting module (Becker & Hickl GmbH, SPC-600).

RESULTS AND DISCUSSION

Thioflavin T Decomposition. Commercial ThT was subjected to two HPLC purification steps to ensure purity, and the chromatogram of the final material is shown in Figure 1. Pure ThT eluted at ∼19.0 min. However, when pure ThT powder was kept in a 4 °C fridge for 2 weeks, three main derivatives were found (red line in Figure 1) and this material is referred to as stored ThT. The retention times for these ThT derivatives were 13.9 min (dThT-1), 15.7 min (dThT-2), and 17.6 min (dThT-3). When pure ThT was irradiated in a photoreactor for 60 min, similar decomposition was seen and this material is referred to as irradiated ThT (blue line in Figure 1).

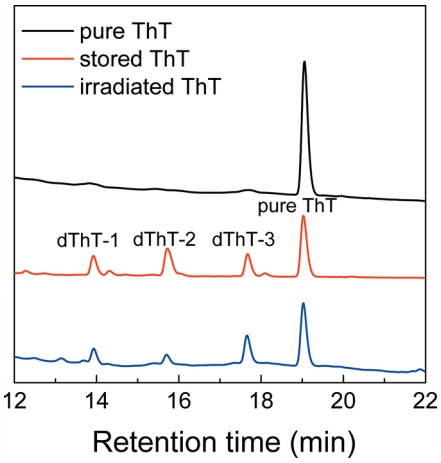

Figure 1. HPLC chromatograms of pure ThT (black line), stored ThT, (red line), and irradiated ThT (blue line). The elution gradient was 0−100% solvent B in 30 min at a flow rate of 3 mL/min. Pure ThT (19.0 min) and its three derivatives, dThT-1 (13.9 min), dThT-2 (15.7 min), and dThT-3 (17.6 min), were resolved by HPLC and the fractions collected. The detection wavelength is 220 nm.

Figure 2A shows the normalized absorption spectra of pure ThT (black), stored ThT (red), and irradiated ThT (blue) in water. The absorption spectrum of pure ThT had an absorption maximum at 412 nm, while the absorption maximum of stored ThT and irradiated ThT were slightly blue-shifted to 410 and 408 nm, respectively. The slight difference in the absorption spectra of the stored and irradiated ThT samples is due to the different ratios of ThT derivatives generated in the two samples. It is worth noting that an absorbance increase at ∼330 nm was seen with both stored and irradiated ThT. The absorbance at this wavelength is a useful indicator of ThT degradation, as the ratio of the absorbance at 412 and 330 nm (A_{412}/A_{330}) of pure ThT and stored ThT is 13.4 and 4.5, respectively.[58]

Structure of the ThT Derivatives. In order to determine the structure of the three ThT derivatives, the molecular formula of ThT and its three derivatives were determined by mass spectroscopy. As shown in Table 1, dThT-3 contained one carbon and two hydrogen atoms less than ThT, suggesting that one of the four methyl groups had been removed from ThT. Similarly, dThT-2 might have lost two methyl groups, since it contained two carbon and four hydrogen atoms less than ThT. By comparison with the one-dimensional nuclear magnetic resonance (1D-NMR) spectrum of purified ThT (Figure S2, Supporting Information), we concluded that dThT-2 had lost two methyl groups from the aminobenzene moiety and dThT-3 one methyl group. The N-demethylation mechanism might be similar to that of an aminoazobenzene dye, AO52.[59] The hydroxyl radical generated upon photoirradiation extracts one electron from the nitrogen atom of the dimethylamino group, and the resulting radical cation is oxidized and forms an iminium ion, from which the methylamino group formed by solvolysis.[60,61] dThT-1 contained one oxygen more and two hydrogens less than ThT, suggesting that it might be a product of oxidation. The 1D-NMR spectrum of dThT-1 was too complicated to resolve (data not shown) because it is unstable in water during spectrum recording.

dx.doi.org/10.1021/jp309331u | J. Phys. Chem. B 2013, 117, 3459−3468

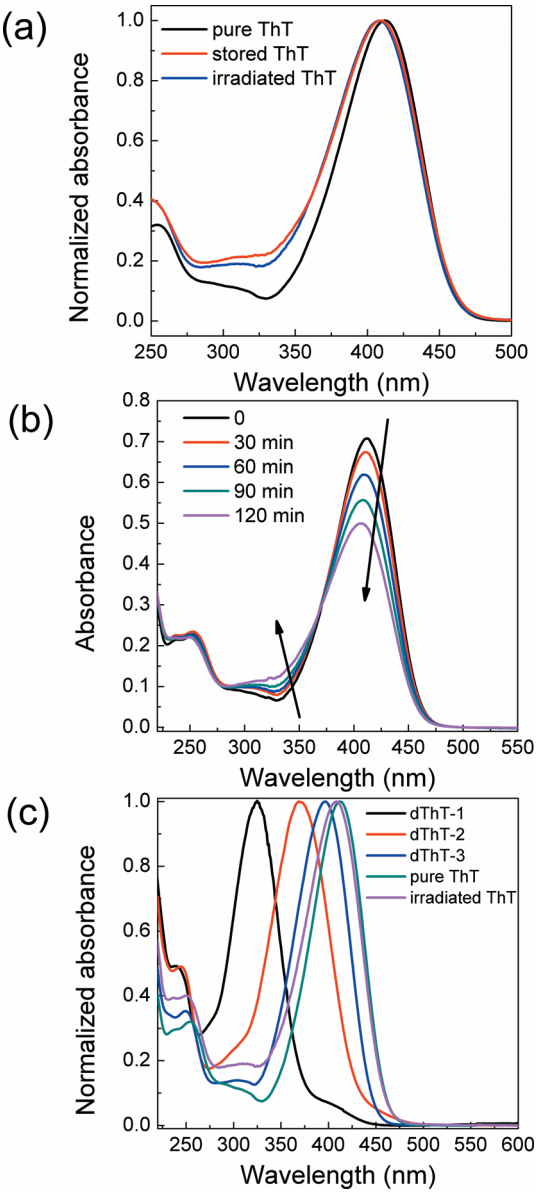

Figure 2. Effect of storage or photoirradiation of ThT on the absorption spectrum. (a) Normalized absorption spectra of pure ThT (black), stored ThT (red), and irradiated ThT (blue). (b) Absorption spectra of pure ThT (20 μM) before irradiation (black) and after irradiation for 30 (red), 60 (blue), 90 (green), or 120 (purple) min. The arrows indicate the direction of spectrum shifting. (c) Normalized absorption spectra of dThT-1 (black), dThT-2 (red), dThT-3 (blue), purified ThT (green), and irradiated ThT (purple). Absorption spectra in parts a and c were normalized to the peak value for each sample tested, assigned a value of 1.

Spectroscopic Properties of ThT and Its Derivatives. The UV/vis absorption and fluorescence spectra of ThT and its derivatives were explored in order to understand how oxidation and demethylation affected the spectroscopic properties of ThT. As shown in Figure 2A and B, photoirradiation affected the absorption spectrum of ThT in the range 280−360 nm. ThT and its three derivatives had absorption maxima at different wavelengths, namely, 325 nm for dThT-1, 369 nm for dThT-2, 397 nm for dThT-3, and 412 nm for pure ThT (Figure 2C). The absorption spectrum of dThT-1 showed the largest blue-shift (Figure 2C), suggesting a significant structural difference for dThT-1. A shoulder peak appearing at around 400 nm is due to impurity, as suggested by the excitation spectrum of dThT-1 (data not shown). The results in Figure 2B and C suggest that the increased absorption of irradiated ThT in the short wavelength range (280−360 nm) is mainly due to the contributions of dThT-1 and dThT-2.

Table 1. Molecular Formula, Absorption and Emission Maxima, and Normalized Fluorescence Enhancement Factor upon Amyloid Binding for Pure ThT and Its Derivatives

	molecular formula	absorption maximum (nm)	fluorescence maximum (nm)		normalized fluorescence enhancement factor
			without fibril in DI	with fibril in DI	
ThT	$C_{17}H_{19}N_2S$	412	487	478	100
dThT-1	$C_{17}H_{17}N_2OS$	325	446	446	
dThT-2	$C_{15}H_{15}N_2S$	370	456	456	4.5
dThT-3	$C_{16}H_{17}N_2S$	397	465	465	63.6

Impurities in commercial ThT can be removed by recrystallization.[27,29] Voropai and colleagues suggested that the absorption in the 300−350 nm region is due to impurities in the ThT preparation. They found that the intensity ratio (I_{340}/I_{420}) of the ThT excitation spectrum (monitored at 480 nm) decreased after recrystallization from an acetonitrile/ethanol mixture[58] and suggested that this excitation was not an intrinsic fluorescence property of ThT but comes from impurities. On the basis of our results *vide supra*, the absorption signal change in the 300−350 nm region might be the result of a ThT modification.

The emission spectra of pure and irradiated ThT measured in deionized water are shown in Figure 3A. When excited at 350 nm, irradiated ThT showed strong fluorescence intensity at 450 nm, whereas no emitted fluorescence was observed for pure ThT except for the Raman signal of water at 397 nm. These data show that the characteristic fluorescence peak at 450 nm comes from the ThT derivatives and not from pure ThT. To determine which derivative contributed the emission at 450 nm, irradiated ThT was analyzed by HPLC (Figure 3B). Since there is an isosbestic point at 370 nm (Figure 2B), the percentages of dThT-1, dThT-2, and dThT-3 after irradiating pure ThT for 60 min were estimated on the basis of the absorbance at 370 nm. The product yield was 1.1% (dThT-1), 2.4% (dThT-2), and 26.8% (dThT-3), showing that nearly one-third of the pure ThT was degraded. Interestingly, only dThT-1, the oxidized derivative, showed fluorescence at 450 nm after excitation at 350 nm (Figure 3B). Some reports have suggested that the ThT monomer emits fluorescence centered at 450 nm, but not 480 nm, when excited at 330 nm and that the emission peak at 480 nm when excited at 412 nm is due to ThT aggregation.[28−31,58] Our data suggest that the emission peak at 450 nm comes from oxidized ThT.

Photophysics of ThT and Its Derivatives on Binding to Amyloid Fibrils. To investigate the effect of ThT modifications on the spectroscopic properties of the dye−fibril complex, the fluorescence spectra of pure ThT and its derivatives in the absence or presence of amyloid fibrils were recorded by exciting at the absorption maximum of each dye (Figure 4). The characteristic peaks in the absorption and fluorescence spectra are summarized in Table 1. No fluorescence enhancement could be observed when dThT-1 was mixed with insulin fibrils, and the slightly lower

dx.doi.org/10.1021/jp309331u | J. Phys. Chem. B 2013, 117, 3459−3468

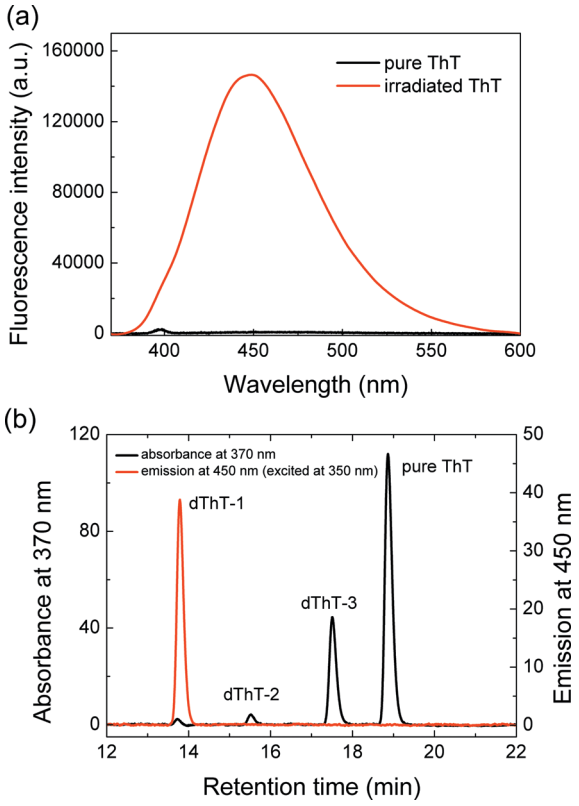

Figure 3. Effect of photoirradiation on the ThT fluorescence spectrum and HPLC profile of ThT. (a) Fluorescence emission spectra recorded with excitation at 350 nm for pure and irradiated ThT. (b) HPLC profile of irradiated ThT monitored by absorbance at 370 nm (black) and fluorescence emission at 450 nm when excited at 350 nm (red). An elution gradient of 0−100% solvent B in 30 min and a flow rate of 3 mL/min were used.

fluorescence intensity of the dThT-1/fibril complex compared to dThT-1 alone might be due to light scattering by the fibrils (Figure 4A). In contrast, dThT-2 (Figure 4B), dThT-3 (Figure 4C), and ThT (Figure 4D) all showed weak fluorescence in water and significant fluorescence enhancement was seen for all three dyes after binding to fibrils. ThT has the largest fluorescence increase. To compare the fluorescence enhancement effect of ThT, dThT-2, and dThT-3, the integrated fluorescence intensity in the presence of fibrils was divided by the integrated fluorescence intensity in the absence of fibrils and the resulting "enhancement ratio" ($F_{\text{fibril}}/F_{\text{no fibril}}$) was plotted against the added fibril amount (Figure 5). The slope of each line in Figure 5 represents the fluorescence enhancement factor of each dye. We normalized the fluorescence enhancement factor of ThT as 100, and the factor for dThT-2 and dThT-3 was calculated as 4.5 and 63.6, respectively. The data is summarized in Table 1 as well.

Our experimental results showed a lower fluorescence enhancement effect for all ThT derivatives compared to ThT. To check whether amyloid-binding ability affects the fluorescence enhancement factor, ThT and its derivatives were mixed with the same amount of insulin fibrils, and then, the solutions were centrifuged at 16 100*g* for 30 min at room temperature. The UV spectra of the unbound dyes were compared with those of the dye solutions before adding fibrils (Figure 6). It is evident that dThT-1 hardly bound to the insulin fibrils and hence no fluorescence intensity increase could be observed in the presence of amyloid fibrils (Figure 4A). According to the UV spectra in Figure 6, the amyloid-binding ratio for ThT, dThT-2, and dThT-3 is 33, 10, and 33%, respectively. Losing one methyl group (dThT-3) did not affect the amyloid-binding ability, but losing two methyl groups (dThT-2) decreased two-thirds of the amyloid-binding ability. Since dThT-3 has the same amyloid-binding ratio as ThT, amyloid-binding ability is not the only factor affecting the fluorescence enhancement effect of the ThT derivatives.

The fluorescence lifetimes of ThT, dThT-2, and dThT-3 after binding with insulin fibrils were measured (Figure 7). The lifetime of free ThT is very fast (<1 ps),[38,45,62,63] and the fluorescence decay trace of ThT shown in the figure represents our instrument response function. The fluorescence decay traces of ThT, dThT-2, and dThT-3 after binding with insulin fibrils were fitted with a single exponential equation. Our results showed that they have very similar fluorescence lifetimes of ~1.85 ns. Fluorescence lifetime is equal to $1/(k_r + k_{nr})$; k_r is the radiative decay rate and k_{nr} is the nonradiative decay rate. Our fluorescence lifetime data suggested that values of $k_r + k_{nr}$ for ThT, dThT-2, and dThT-3 are similar. The comparison of fluorescence enhancement in Figure 5 suggested that k_r (ThT) > k_r (dThT-3) > k_r (dThT-2). Therefore, losing the methyl group in the dimethylaminobenzene ring should increase the nonradiative decay rate of ThT. The "molecular rotor" model proposes that the increase in the Q.Y. of ThT on binding to amyloid is due to rotational restriction of the benzothiazole and dimethylaminobenzene rings of ThT.[36,40,45,48,63] If the rotation to the TICT state is delayed long enough, radiative decay from the LE state is able to occur. In the case of the demethylated derivatives, dThT-2 and dThT-3, the loss of methyl group(s) could reduce the interaction between the benzene group and the local environment. We speculate that, inside the dye binding pocket, dThT-2 and dThT-3 are able to rotate more quickly from the LE to the TICT state than ThT due to the reduced interaction. Consequently, dThT-2 and dThT-3 would have a lower fluorescence Q.Y. than ThT in the dye/amyloid complex.

Computational Excited Potential Energy Surface of ThT and Its Derivatives. In the "molecular rotor" model, fluorescence emission occurs on going from the LE state to the ground state, whereas fluorescence quenching occurs on going from the fluorescent LE state to the nonfluorescent TICT state and further to the ground state. To gain insight into this process, it was necessary to map the excited state potential energy surface. Instead of computing the entire multidimensional potential energy surface, a reduced potential energy surface corresponding to a single important degree of freedom was computed. The most relevant degree of freedom describing the conversion from the LE to the TICT is the rotation around the dihedral angle defined along the C−C bond connecting the benzothiazole and dimethylaminobenzene rings (Figure 8). This dihedral angle was identified in earlier computational work as the relevant twisting angle.[48,64,65] A relaxed coordinate scan of this dihedral angle was performed, with the dihedral angle defined using the sulfur atom of the benzothiazole ring. The goal was to determine whether the potential energy surface could explain the difference in the fluorescence of ThT and its two derivatives. A larger energy barrier separating the LE and TICT states on the ThT potential energy surface would explain why a larger fluorescence enhancement factor was observed with ThT than the derivatives.

dx.doi.org/10.1021/jp309331u | J. Phys. Chem. B 2013, 117, 3459−3468

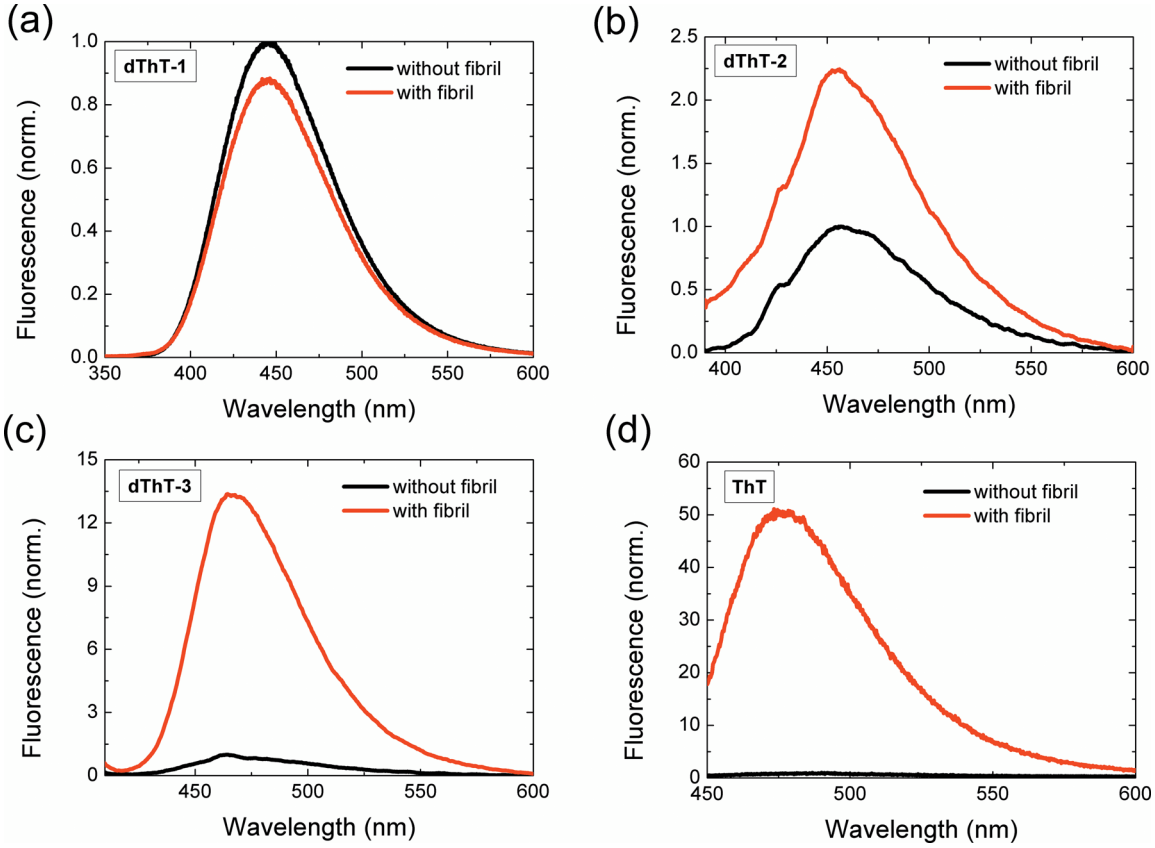

Figure 4. The fluorescence spectra of dThT-1, dThT-2, dThT-3, and pure ThT in the absence (black) and presence (red) of the same amount of insulin fibrils. The fluorescence intensity of each sample in the absence of fibrils was normalized as "1". The spectra were recorded with excitation at the absorption maximum of each sample (see Figure 2c).

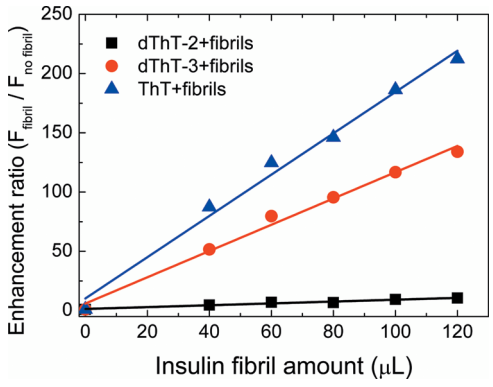

Figure 5. Comparison of the fluorescence enhancement effect of ThT, dThT-2, and dThT-3. The same concentrations of ThT, dThT-2, and dThT-3 were mixed with different amounts of insulin fibrils. The fluorescence spectra of the samples were recorded with excitation at 440 nm. The emission peak between 450 and 600 nm was integrated. The integrated fluorescence intensity in the presence of fibrils was divided by the integrated fluorescence intensity in the absence of fibrils, and the resulting "enhancement ratio" ($F_{fibril}/F_{no\ fibril}$) is shown in the *y*-axis.

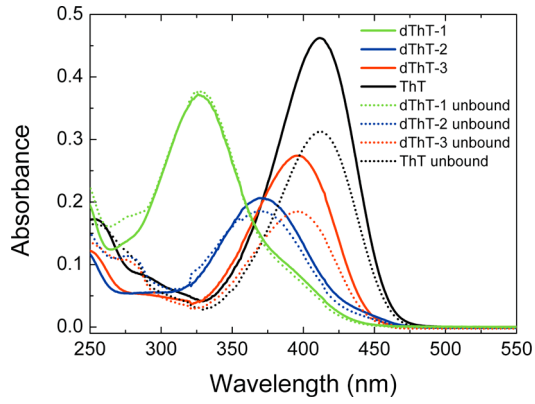

Figure 6. Amyloid-binding ability of dThT-1, dThT-2, dThT-3, and ThT. These four dyes were dissolved in water. Their UV spectra were recorded (solid line). After adding the same amount of insulin fibrils, the solutions were centrifuged. The unbound dyes were remained in the supernatants, and the UV spectra of the supernatants were recorded (dotted line).

Figure 8A compares the amount of charge held on the aminobenzene ring of ThT and the two derivatives dThT-2 and dThT-3 in the first excited state. The amount of positive charge for ThT and both of its derivatives increased rapidly with increasing dihedral angle, consistent with increased charge transfer between the donor and acceptor moieties. In contrast, the amount of charge held on the aminobenzene ring in the ground state and other excited states remained almost constant as φ was rotated (Figure S4, Supporting Information). Figure 8B shows the oscillator strength between the S_0 and S_1 states along the φ angle scan. The oscillator strength for all three complexes was weaker in the TICT state ($\varphi = 90°$) than in the LE state ($\varphi = 30°$), showing that emission is less likely from the TICT state than the LE state. The ordering of the oscillator strengths is ThT > dThT-3 > dThT-2, indicating that loss of methyl groups results in a slightly reduced rate of emission.

dx.doi.org/10.1021/jp309331u | J. Phys. Chem. B 2013, 117, 3459−3468

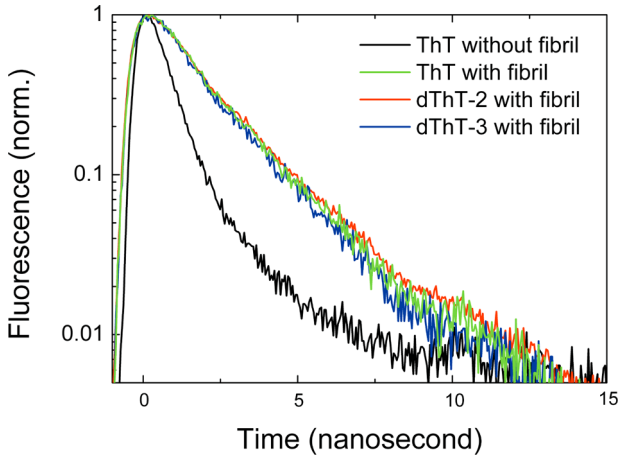

Figure 7. Time-dependent fluorescence intensity decay of free ThT (black), ThT bound to the insulin fibrils (green), dThT-2 bound to the insulin fibrils (red), and dThT-3 bound to the insulin fibrils (blue) for fluorescence lifetime measurement.

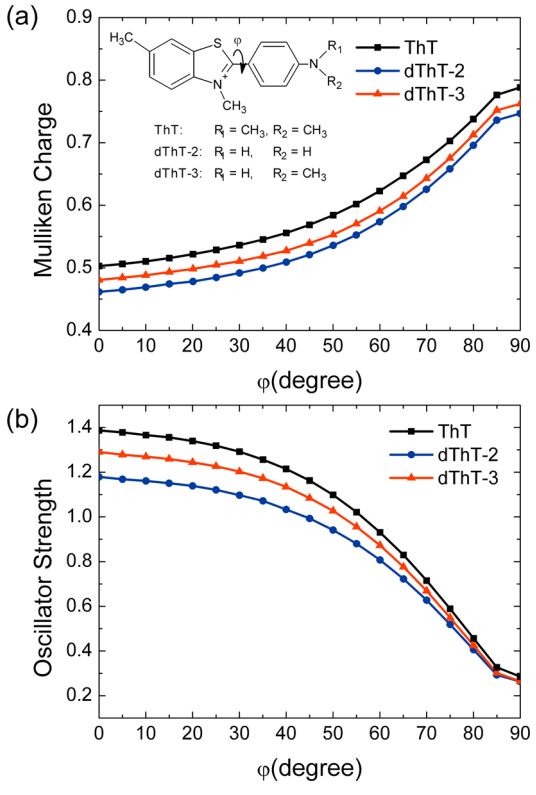

Figure 8. Charge of the aminobenzene ring (a) and gas phase oscillator strength (b) of the S1 state of ThT (black squares) and its two derivatives dThT-2 (blue circles) and dThT-3 (red triangles) computed at the CIS/6-31G** level along a relaxed geometry scan of the φ dihedral angle. Molecular structures of ThT and its derivatives, dThT-2 and dThT-3, are shown in part a.

Figure 9A shows the gas phase potential energy surface for the first (S_1) excited state. A single minimum energy structure at $\varphi = 30°$ was observed for ThT, dThT-2, and dThT-3. Figure 9B shows the S_1 potential energy surface when an implicit solvation model described by a dielectric constant (ε) of 80, approximately the dielectric constant of water, was included in the computation. As expected, the solvation energy in the high dielectric environment shifted the energy of the $\varphi = 90°$

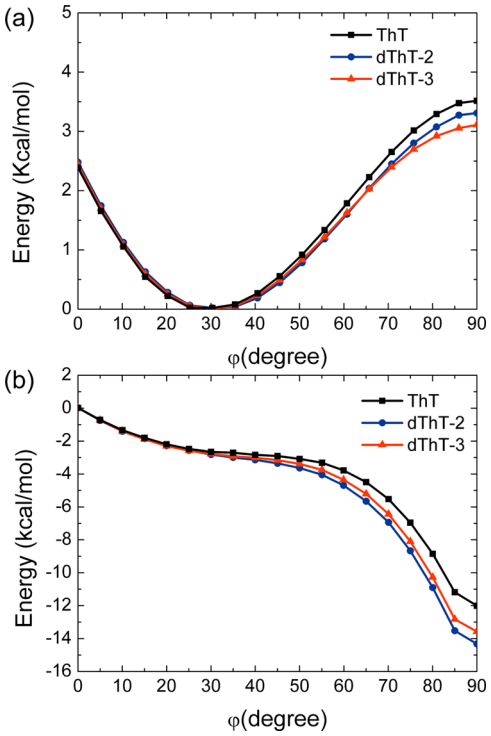

Figure 9. S1 potential energy surface of ThT (black squares) and its two derivatives dThT-2 (blue circles) and dThT-3 (red triangles) computed in a vacuum (a) or using an implicit solvation model with a dielectric constant of 80 (b) at the CIS/6-31G** level along a relaxed geometry scan of the φ dihedral angle.

conformer to a lower energy than the $\varphi = 30°$ conformer. This shows that, in a high dielectric solvent, such as water, the transition from the LE state to the TICT state is barrier-less. The potential energy surfaces for ThT and its two derivatives, dThT-2 and dThT-3, shared the same profile between angles of 0 and 40°, the only noticeable difference being that the energy of the TICT state was lower for the derivatives. The dielectric continuum solvation model used here accounts only for the electrostatic contributions to the solvation energy and neglects other terms that may be important, for example, steric interactions with a viscous environment.

Since the TICT state of ThT has been investigated previously using quantum chemical computation,[48,64−66] it is important to compare the results of this work with those of the earlier studies. An important difference with the earlier work is that the potential energy surface was previously computed using the semiempirical INDO/S method using excited state geometries obtained from the CIS/3-21G level.[64] We believe that the larger 6-31G** basis set employed in our study provides a more accurate prediction of the excited state geometry. The results using the INDO/S method predicted a barrier-less transition from the LE state to the TICT state for ThT in the gas phase and a minimum energy conformation corresponding to $\varphi = 90°$. In our study, we found that $\varphi = 90°$ was not a minimum on the gas phase potential energy surface and that the minimum was actually at $\varphi = 30°$ (see Figure 9A). However, we did find a barrier-less transition when the effect of solvation was included in the calculation.

Kinetics of Insulin Fibril Formation Traced Using Pure or Irradiated ThT. When ThT solutions (20 μM) without (Figure 10A) or with (Figure 10B) previous irradiation were used to study the kinetics of insulin fibril formation by

dx.doi.org/10.1021/jp309331u | J. Phys. Chem. B 2013, 117, 3459−3468

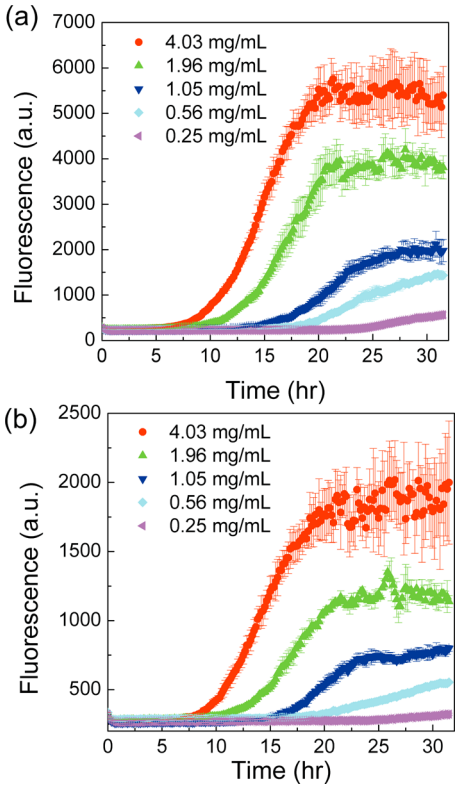

Figure 10. Kinetics of insulin fibril formation measured using pure ThT (a) or irradiated ThT (b). Insulin was dissolved in fibrillization buffer at different concentrations (indicated in each panel), mixed with an equal volume of 20 μM pure ThT or irradiated ThT, and incubated at 45 °C for the indicated time. The fluorescence intensity at 478 nm was monitored with excitation at 412 nm.

observing the fluorescence intensity at 478 nm with excitation at 412 nm, the results showed that the fluorescence intensity was 3 times higher when pure ThT was used, suggesting that fluorescence measurement in the ThT binding assay could be affected by the quality of the ThT. However, as shown in Figure 11, the lag time in the fibrillization kinetics was not affected. In addition, when the lag times obtained by fitting the kinetic traces in Figure 10 were plotted versus insulin concentration, an inverse correlation between protein concentration and lag time could be clearly seen and this was not affected by the quality of the ThT.

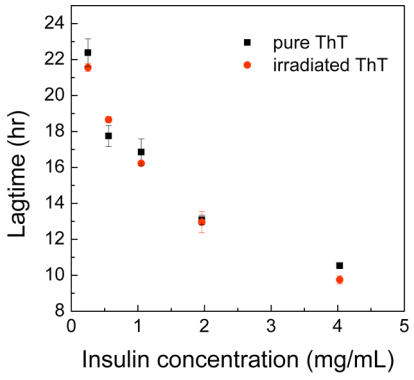

Figure 11. Plot of lag time of fibrillization versus insulin concentration using pure ThT (black squares) or irradiated ThT (red circles).

CONCLUSION

We found that pure ThT is degraded into three kinds of derivatives during storage or by UV irradiation. An oxidative derivative, dThT-1, shows a high fluorescence Q.Y. and a characteristic emission peak at 450 nm when excited at 330 nm. The results revealed that the ThT emission at 450 nm comes from dThT-1, rather than monomeric ThT, as reported previously. In addition, dThT-1 displays very different photophysics to pure ThT and the other two derivatives and could not bind to amyloid fibrils. The derivatives dThT-2 and dThT-3 are N-demethylation products, which have lost two and one methyl groups from the aminobenzene moiety, respectively. The fluorescence enhancement observed after binding to amyloid fibrils follows the order pure ThT > dThT-3 > dThT-2 and correlates with the number of methyl groups on the aminobenzene ring. Quantum chemical calculations showed that the methyl groups did not alter the excited state potential energy surface and predicted the same TICT photophysics for ThT and its derivatives. These results suggest that, in the "molecular rotor" model, the interaction of the methyl groups in the aminobenzene moiety with the amyloid fibril binding pocket helps delay rotation to the TICT state and the loss of methyl group(s) increases of the nonradiative decay rate and decreases of radiative decay rate. Moreover, losing two methyl groups significantly decreases the amyloid-binding ability of dThT-2. Therefore, the fluorescence enhancement effects of dThT-2 and dThT-3 upon binding with amyloid fibrils are much lower than that of pure ThT. Finally, ThT degradation does not affect the lag time measurement when studying fibrillization kinetics, though the observed fluorescence intensity is markedly decreased.

ASSOCIATED CONTENT

Supporting Information

Figure S1: Extinction coefficient measurement of pure ThT. Figure S2: 1D NMR of pure ThT, dThT-2, and dThT-3. Figure S3: Fluorescence quantum yield measurement of pure ThT, dThT-1, dThT-2, and dThT-3. Figure S4: Charge calculation of the ground state and excited states of ThT. This material is available free of charge via the Internet at http://pubs.acs.org.

AUTHOR INFORMATION

Corresponding Author

*Address: Institute of Biological Chemistry, Academia Sinica, No. 128, Sec. 2, Academia Rd, Nankang, Taipei, 11529, Taiwan. Phone: +(886)-2-2785-5696. Fax: +(886)-2-2788-9759. E-mail: pyc@gate.sinica.edu.tw.

Author Contributions

‖J.C.-C.H., E.H.-L.C.: These authors made equal contributions.

Notes

The authors declare no competing financial interest.

ACKNOWLEDGMENTS

We are grateful to the staff of the TCX-D800 Metabolomics Core, Technology Commons, College of Life Science, National Taiwan University, for the LC-ESI-MS analysis. This work was supported by the National Science Council, Taiwan, R. O. C. (grant number NSC 100-2321-B-001-026). R.C.S. and C.-P.H. acknowledge support from the Academia Sinica.

REFERENCES

(1) Chiti, F.; Dobson, C. M. Protein Misfolding, Functional Amyloid, and Human Disease. *Annu. Rev. Biochem.* **2006**, *75*, 333−366.

(2) Bucciantini, M.; Giannoni, E.; Chiti, F.; Baroni, F.; Formigli, L.; Zurdo, J. S.; Taddei, N.; Ramponi, G.; Dobson, C. M.; Stefani, M. Inherent Toxicity of Aggregates Implies a Common Mechanism for Protein Misfolding Diseases. *Nature* **2002**, *416*, 507−511.

(3) Collinge, J.; Clarke, A. R. A General Model of Prion Strains and Their Pathogenicity. *Science* **2007**, *318*, 930−936.

(4) Baskakov, I. V.; Legname, G.; Baldwin, M. A.; Prusiner, S. B.; Cohen, F. E. Pathway Complexity of Prion Protein Assembly into Amyloid. *J. Biol. Chem.* **2002**, *277*, 21140−21148.

(5) Pepys, M. B. Amyloidosis. *Annu. Rev. Med.* **2006**, *57*, 223−241.

(6) Buell, A. K.; Dobson, C. M.; Knowles, T. P. J.; Welland, M. E. Interactions between Amyloidophilic Dyes and Their Relevance to Studies of Amyloid Inhibitors. *Biophys. J.* **2010**, *99*, 3492−3497.

(7) DeMarco, M. L.; Daggett, V. From Conversion to Aggregation: Protofibril Formation of the Prion Protein. *Proc. Natl. Acad. Sci. U.S.A.* **2004**, *101*, 2293−2298.

(8) Dickinson, W. H. On the Nature of the Waxy, Lardaceous, or Amyloid Deposit. *Med. Chir. Trans.* **1867**, *50*, 39−56.

(9) Ladewig, P. Double-Refringence of the Amyloid-Congo-Red-Complex in Histological Sections. *Nature* **1945**, *156*, 81−82.

(10) Kelenyi, G. Thioflavin S Fluorescent and Congo Red Anisotropic Stainings in the Histologic Demonstration of Amyloid. *Acta Neuropathol.* **1967**, *7*, 336−348.

(11) Chang, E. S.; Liao, T. Y.; Lim, T. S.; Fann, W.; Chen, R. P. A New Amyloid-Like β-Aggregate with Most of the Amyloid Characteristics except Fibril Morphology. *J. Mol. Biol.* **2009**, *385*, 1257−1265.

(12) Chen, A. K.; Lin, R. Y.; Hsieh, E. Z.; Tu, P. H.; Chen, R. P.; Liao, T. Y.; Chen, W.; Wang, C. H.; Huang, J. J. Induction of Amyloid Fibrils by the C-Terminal Fragments of TDP-43 in Amyotrophic Lateral Sclerosis. *J. Am. Chem. Soc.* **2010**, *132*, 1186−1187.

(13) Chen, P. Y.; Lin, C. C.; Chang, Y. T.; Lin, S. C.; Chan, S. I. One O-Linked Sugar Can Affect the Coil-to-Beta Structural Transition of the Prion Peptide. *Proc. Natl. Acad. Sci. U.S.A.* **2002**, *99*, 12633−12638.

(14) Ho, C. C.; Lee, L. Y.; Huang, K. T.; Lin, C. C.; Ku, M. Y.; Yang, C. C.; Chan, S. I.; Hsu, R. L.; Chen, R. P. Tuning the Conformational Properties of the Prion Peptide. *Proteins: Struct., Funct., Bioinf.* **2009**, *76*, 213−225.

(15) Lee, L. Y.; Chen, R. P. Quantifying the Sequence-Dependent Species Barrier between Hamster and Mouse Prions. *J. Am. Chem. Soc.* **2007**, *129*, 1644−1652.

(16) Liao, T. Y.; Lee, L. Y.; Chen, R. P. Leu-138 in the Bovine Prion Peptide Fibrils Is Involved in the Seeding Discrimination Related to Codon-129 M/V Polymorphism in the Prion Peptide Seeding Experiment. *FEBS J.* **2011**, *278*, 4351−4361.

(17) Zhao, D. S.; Chen, Y. X.; Liu, Q.; Zhao, Y. F.; Li, Y. M. Exploring the Binding Mechanism of Thioflavin-T to the Beta-Amyloid Peptide by Blind Docking Method. *Sci. China: Chem.* **2012**, *55*, 112−117.

(18) Toyama, B. H.; Weissman, J. S. Amyloid Structure: Conformational Diversity and Consequences. *Annu. Rev. Biochem.* **2011**, *80*, 557−585.

(19) Makin, O. S.; Serpell, L. C. Structures for Amyloid Fibrils. *FEBS J.* **2005**, *272*, 5950−5961.

(20) Ostapchenko, V.; Gasset, M.; Baskakov, I. V. Atomic Force Fluorescence Microscopy in the Characterization of Amyloid Fibril Assembly and Oligomeric Intermediates. *Methods Mol. Biol.* **2012**, *849*, 157−167.

(21) Ostapchenko, V. G.; Sawaya, M. R.; Makarava, N.; Savtchenko, R.; Nilsson, K. P.; Eisenberg, D.; Baskakov, I. V. Two Amyloid States of the Prion Protein Display Significantly Different Folding Patterns. *J. Mol. Biol.* **2010**, *400*, 908−921.

(22) Ban, T.; Hamada, D.; Hasegawa, K.; Naiki, H.; Goto, Y. Direct Observation of Amyloid Fibril Growth Monitored by Thioflavin T Fluorescence. *J. Biol. Chem.* **2003**, *278*, 16462−16465.

(23) Naiki, H.; Higuchi, K.; Hosokawa, M.; Takeda, T. Fluorometric Determination of Amyloid Fibrils in Vitro Using the Fluorescent Dye, Thioflavin T1. *Anal. Biochem.* **1989**, *177*, 244−249.

(24) Bhasikuttan, A. C.; Choudhury, S. D.; Pal, H.; Mohanty, J. Supramolecular Assemblies of Thioflavin T with Cucurbiturils: Prospects of Cooperative and Competitive Metal Ion Binding. *Isr. J. Chem.* **2011**, *51*, 634−645.

(25) Sulatskaya, A. I.; Maskevich, A. A.; Kuznetsova, I. M.; Uversky, V. N.; Turoverov, K. K. Fluorescence Quantum Yield of Thioflavin T in Rigid Isotropic Solution and Incorporated into the Amyloid Fibrils. *PLoS One* **2010**, e15385.

(26) Sen, P.; Fatima, S.; Ahmad, B.; Khan, R. H. Interactions of Thioflavin T with Serum Albumins: Spectroscopic Analyses. *Spectrochim. Acta, Part A* **2009**, *74*, 94−99.

(27) Groenning, M.; Olsen, L.; van de Weert, M.; Flink, J. M.; Frokjaer, S.; Jorgensen, F. S. Study on the Binding of Thioflavin T to Beta-Sheet-Rich and Non-Beta-Sheet Cavities. *J. Struct. Biol.* **2007**, *158*, 358−369.

(28) Naik, L. R.; Naik, A. B.; Pal, H. Steady-State and Time-Resolved Emission Studies of Thioflavin-T. *J. Photochem. Photobiol., A* **2009**, *204*, 161−167.

(29) Ilanchelian, M.; Ramaraj, R. Emission of Thioflavin T and Its Control in the Presence of DNA. *J. Photochem. Photobiol., A* **2004**, *162*, 129−137.

(30) Raj, C. R.; Ramaraj, R. Influence of Cyclodextrin Complexation on the Emission of Thioflavin T and Its Off-On Control. *J. Photochem. Photobiol., A* **1999**, *122*, 39−46.

(31) Raj, C. R.; Ramaraj, R. Emission of Thioflavin T and Its Off-On Control in Polymer Membranes. *Photochem. Photobiol.* **2001**, *74*, 752−759.

(32) Raj, C. R.; Ramaraj, R. Gamma-Cyclodextrin Induced Intermolecular Excimer Formation of Thioflavin T. *Chem. Phys. Lett.* **1997**, *273*, 285−290.

(33) Rodriguez-Rodriguez, C.; Rimola, A.; Rodriguez-Santiago, L.; Ugliengo, P.; Alvarez-Larena, A.; Gutierrez-de-Teran, H.; Sodupe, M.; Gonzalez-Duarte, P. Crystal Structure of Thioflavin-T and Its Binding to Amyloid Fibrils: Insights at the Molecular Level. *Chem. Commun.* **2010**, *46*, 1156−1158.

(34) Qin, L. H.; Vastl, J.; Gao, J. M. Highly Sensitive Amyloid Detection Enabled by Thioflavin T Dimers. *Mol. BioSyst.* **2010**, *6*, 1791−1795.

(35) Khurana, R.; Coleman, C.; Ionescu-Zanetti, C.; Carter, S. A.; Krishna, V.; Grover, R. K.; Roy, R.; Singh, S. Mechanism of Thioflavin T Binding to Amyloid Fibrils. *J. Struct. Biol.* **2005**, *151*, 229−238.

(36) Singh, P. K.; Kumbhakar, M.; Pal, H.; Nath, S. Confined Ultrafast Torsional Dynamics of Thioflavin-T in a Nanocavity. *Phys. Chem. Chem. Phys.* **2011**, *13*, 8008−8014.

(37) Hutter, T.; Amdursky, N.; Gepshtein, R.; Elliott, S. R.; Huppert, D. Study of Thioflavin-T Immobilized in Porous Silicon and the Effect of Different Organic Vapors on the Fluorescence Lifetime. *Langmuir* **2011**, *27*, 7587−7594.

(38) Singh, P. K.; Kumbhakar, M.; Pal, H.; Nath, S. Ultrafast Torsional Dynamics of Protein Binding Dye Thioflavin-T in Nanoconfined Water Pool. *J. Phys. Chem. B* **2009**, *113*, 8532−8538.

(39) Kumar, S.; Singh, A. K.; Krishnamoorthy, G.; Swaminathan, R. Thioflavin T Displays Enhanced Fluorescence Selectively inside Anionic Micelles and Mammalian Cells. *J. Fluoresc.* **2008**, *18*, 1199−1205.

(40) Stsiapura, V. I.; Maskevich, A. A.; Kuzmitsky, V. A.; Uversky, V. N.; Kuznetsova, I. M.; Turoverov, K. K. Thioflavin T as a Molecular Rotor: Fluorescent Properties of Thioflavin T in Solvents with Different Viscosity. *J. Phys. Chem. B* **2008**, *112*, 15893−15902.

(41) Amdursky, N.; Erez, Y.; Huppert, D. Molecular Rotors: What Lies Behind the High Sensitivity of the Thioflavin-T Fluorescent Marker. *Acc. Chem. Res.* **2012**, *45*, 1548−1557.

(42) Erez, Y.; Amdursky, N.; Gepshtein, R.; Huppert, D. Temperature and Viscosity Dependence of the Nonradiative Decay Rates of Auramine-O and Thioflavin-T in Glass-Forming Solvents. *J. Phys. Chem. A* **2012**, *116*, 12056−12064.

(43) Amdursky, N.; Gepshtein, R.; Erez, Y.; Huppert, D. Temperature Dependence of the Fluorescence Properties of Thioflavin-T in Propanol, a Glass-Forming Liquid. *J. Phys. Chem. A* **2011**, *115*, 2540−2548.
(44) Amdursky, N.; Gepshtein, R.; Erez, Y.; Koifman, N.; Huppert, D. Pressure Effect on the Nonradiative Process of Thioflavin-T. *J. Phys. Chem. A* **2011**, *115*, 6481−6487.
(45) Stsiapura, V. I.; Maskevich, A. A.; Tikhomirov, S. A.; Buganov, O. V. Charge Transfer Process Determines Ultrafast Excited State Deactivation of Thioflavin T in Low-Viscosity Solvents. *J. Phys. Chem. A* **2010**, *114*, 8345−8350.
(46) Kitts, C. C.; Bout, D. A. V. Near-Field Scanning Optical Microscopy Measurements of Fluorescent Molecular Probes Binding to Insulin Amyloid Fibrils. *J. Phys. Chem. B* **2009**, *113*, 12090−12095.
(47) Wu, C.; Bowers, M. T.; Shea, J. E. On the Origin of the Stronger Binding of Pib over Thioflavin T to Protofibrils of the Alzheimer Amyloid-Beta Peptide: A Molecular Dynamics Study. *Biophys. J.* **2011**, *100*, 1316−1324.
(48) Maskevich, A. A.; Stsiapura, V. I.; Kuzmitsky, V. A.; Kuznetsova, I. M.; Povarova, O. I.; Uversky, V. N.; Turoverov, K. K. Spectral Properties of Thioflavin T in Solvents with Different Dielectric Properties and in a Fibril-Incorporated Form. *J. Proteome Res.* **2007**, *6*, 1392−1401.
(49) Fodera, V.; Librizzi, F.; Groenning, M.; van de Weert, M.; Leone, M. Secondary Nucleation and Accessible Surface in Insulin Amyloid Fibril Formation. *J. Phys. Chem. B* **2008**, *112*, 3853−3858.
(50) Groenning, M. Binding Mode of Thioflavin T and Other Molecular Probes in the Context of Amyloid Fibrils-Current Status. *J. Chem. Biol.* **2010**, *3*, 1−18.
(51) De Ferrari, G. V.; Mallender, W. D.; Inestrosa, N. C.; Rosenberry, T. L. Thioflavin T Is a Fluorescent Probe of the Acetylcholinesterase Peripheral Site That Reveals Conformational Interactions between the Peripheral and Acylation Sites. *J. Biol. Chem.* **2001**, *276*, 23282−23287.
(52) Foresman, J. B.; Headgordon, M.; Pople, J. A.; Frisch, M. J. Toward a Systematic Molecular-Orbital Theory for Excited-States. *J. Phys. Chem.* **1992**, *96*, 135−149.
(53) Dreuw, A.; Head-Gordon, M. Failure of Time-Dependent Density Functional Theory for Long-Range Charge-Transfer Excited States: The Zincbacteriochlorin-Bacterlochlorin and Bacteriochlorophyll-Spheroidene Complexes. *J. Am. Chem. Soc.* **2004**, *126*, 4007−4016.
(54) Stanton, J. F.; Gauss, J.; Ishikawa, N.; Headgordon, M. A Comparison of Single Reference Methods for Characterizing Stationary-Points of Excited-State Potential-Energy Surfaces. *J. Chem. Phys.* **1995**, *103*, 4160−4174.
(55) Subotnik, J. E. Communication: Configuration Interaction Singles Has a Large Systematic Bias against Charge-Transfer States. *J. Chem. Phys.* **2011**, *135*, 071104.
(56) Improta, R.; Barone, V.; Scalmani, G.; Frisch, M. J. A State-Specific Polarizable Continuum Model Time Dependent Density Functional Theory Method for Excited State Calculations in Solution. *J. Chem. Phys.* **2006**, *125*, 054103.
(57) Nielsen, L.; Khurana, R.; Coats, A.; Frokjaer, S.; Brange, J.; Vyas, S.; Uversky, V. N.; Fink, A. L. Effect of Environmental Factors on the Kinetics of Insulin Fibril Formation: Elucidation of the Molecular Mechanism. *Biochemistry* **2001**, *40*, 6036−6046.
(58) Voropai, E. S.; Samtsov, M. P.; Kaplevskii, K. N.; Maskevich, A. A.; Stepuro, V. I.; Povarova, O. I.; Kuznetsova, I. M.; Turoverov, K. K.; Fink, A. L.; Uverskii, V. N. Spectral Properties of Thioflavin T and Its Complexes with Amyloid Fibrils. *J. Appl. Spectrosc.* **2003**, *70*, 868−874.
(59) Galindo, C.; Jacques, P.; Kalt, A. Photodegradation of the Aminoazobenzene Acid Orange 52 by Three Advanced Oxidation Processes: UV/H_2O_2 UV/TiO_2 and VIS/TiO_2 - Comparative Mechanistic and Kinetic Investigations. *J. Photochem. Photobiol., A* **2000**, *130*, 35−47.
(60) Watanabe, T.; Takizawa, T.; Honda, K. Photocatalysis through Excitation of Adsorbates. 1. Highly Efficient N-Deethylation of Rhodamine B Adsorbed to Cadmium Sulfide. *J. Phys. Chem.* **1977**, *81*, 1845−1851.
(61) Nikogosyan, D.; Angelov, D. Formation of Free Radicals in Water under High-Power Laser UV Irradiation. *Chem. Phys. Lett.* **1981**, *77*, 208−210.
(62) Mohanty, J.; Barooah, N.; Dhamodharan, V.; Harikrishna, S.; Pradeepkumar, P. I.; Bhasikuttan, A. C. Thioflavin T as an Efficient Inducer and Selective Fluorescent Sensor for the Human Telomeric G-Quadruplex DNA. *J. Am. Chem. Soc.* **2013**, *135*, 367−376.
(63) Singh, P. K.; Kumbhakar, M.; Pal, H.; Nath, S. Viscosity Effect on the Ultrafast Bond Twisting Dynamics in an Amyloid Fibril Sensor: Thioflavin-T. *J. Phys. Chem. B* **2010**, *114*, 5920−5927.
(64) Stsiapura, V. I.; Maskevich, A. A.; Kuzmitsky, V. A.; Turoverov, K. K.; Kuznetsova, I. M. Computational Study of Thioflavin T Torsional Relaxation in the Excited State. *J. Phys. Chem. A* **2007**, *111*, 4829−4835.
(65) Wolfe, L. S.; Calabrese, M. F.; Nath, A.; Blaho, D. V.; Miranker, A. D.; Xiong, Y. Protein-Induced Photophysical Changes to the Amyloid Indicator Dye Thioflavin T. *Proc. Natl. Acad. Sci. U.S.A.* **2010**, *107*, 16863−16868.
(66) Huppert, D.; Erez, Y.; Liu, Y. H.; Amdursky, N. Modeling the Nonradiative Decay Rate of Electronically Excited Thioflavin T. *J. Phys. Chem. A* **2011**, *115*, 8479−8487.